



The effect of diluent on flame structure and laminar burning speeds of JP-8/oxidizer/diluent premixed flames

Kian Eisazadeh-Far^a, Ali Moghaddas^a, Hameed Metghalchi^{a,*}, James C. Keck^b

^a Northeastern University, Boston, MA 02115, USA

^b Massachusetts Institute of Technology, Cambridge, MA 02139, USA

ARTICLE INFO

Article history:

Received 10 June 2010

Received in revised form 5 November 2010

Accepted 15 November 2010

Available online 30 November 2010

This paper is dedicated to the memory of Professor James C. Keck (1924–2010), MIT. The authors are indebted to Professor James C. Keck who was an invaluable source of scientific feedback to our group during past years. He was also our coauthor in this paper and passed away on August 2010 when this manuscript was under review.

Keywords:

JP-8

Laminar burning speed

Combustion instability

Diluent

ABSTRACT

Experimental studies have been performed to investigate the flame structure and laminar burning speed of JP-8/oxidizer/diluent premixed flames at high temperatures and pressures. Three different diluents including argon, helium, and a mixture of 14% CO₂ and 86% N₂ (extra diluent gases), were used. The experiments were carried out in two constant volume spherical and cylindrical vessels. Laminar burning speeds were measured using a thermodynamics model based on the pressure rise method. Temperatures from 493 to 700 K and pressures from 1 to 11.5 atm were investigated. Extra diluent gases (EDG) decrease the laminar burning speeds but do not greatly impact the stability of the flame compared to JP-8/air. Replacing nitrogen in the air with argon and helium increases the range of temperature and pressure in the experiments. Helium as a diluent also increases the temperature and pressure range of stable flame as well as the laminar burning speed. Power law correlations have been developed for laminar burning speeds of JP-8/air/EDG and JP-8/oxygen/helium mixtures at a temperature range of 493–700 K and a pressure range of 1–10 atm for lean mixtures.

© 2010 Elsevier Ltd. All rights reserved.

1. Introduction

Jet Propellant-8 (JP-8) is a fuel currently used in land based engines and aviation combustors. It would be beneficial to extend the application of this fuel under the framework of the “Single Fuel Concept” [1]. There are several theoretical studies underway to develop the chemical kinetics mechanisms of this complex fuel. Validation of these mechanisms requires reliable and highly accurate experimental data. These experimental data should be available in a wide range of temperatures, pressures and equivalence ratios. Laminar burning speed, which is a fundamental property of each fuel, can be used to provide experimental data for chemical kinetics mechanisms. It is also used for the correlation of turbulent flame propagation in internal combustion engines. Currently some experimental and theoretical data exist in the literature about the laminar burning speeds of JP-8 fuel at atmospheric pressures and high temperatures [2–4]. Ji et al. [2] measured the laminar burning

speed at a temperature of 403 K and atmospheric pressure. They used a counter-flow flame experimental facility to estimate the laminar burning speeds after stretch corrections. Kumar et al. [3] measured the laminar burning speeds of Jet-A fuels and other heavy hydrocarbons at a temperature of 470 K and atmospheric pressure by a counter-flow flame similar to Ji et al. These data are reported in a limited range of temperatures and pressures. In most combustors, such as internal combustion engines, fuel is burned at high temperatures and pressures; therefore the measurement of laminar burning speeds under those conditions is essential.

Eisazadeh-Far et al. [5] measured the laminar burning speeds of JP-8/air mixtures at a temperature range of 500–700 K, pressures of 1–6 atm and equivalence ratios of 0.8–1. They concluded that JP-8/air flames are sensitive to instability at high pressures and richer mixtures. Burning speeds for smooth flames were measured by the pressure rise method and a power law fit correlation for laminar burning speed calculation was developed.

This paper investigates the effect of diluent type on the stability and laminar burning speeds of JP-8/air/EDG and JP-8/oxygen/ (argon and helium) flames. The effect of EDG (extra diluent gases) addition to JP-8/air on flame structure will be studied in a wide range of temperatures, pressures and equivalence ratios. Following

* Corresponding author. Address: Mechanical and Industrial Engineering, 334 Snell Engineering Center, Northeastern University, 360 Huntington Avenue, Boston, MA 02115, USA. Tel.: +1 617 373 2973; fax: +1 617 373 2921.

E-mail address: metghalchi@coe.neu.edu (H. Metghalchi).

the flame structure study, laminar burning speeds of JP-8/air/EDG and JP-8/oxygen/helium will be reported at temperatures of (493–700 K) and higher pressures (1–10 atm). It will be shown that laminar burning speeds of JP-8/oxygen/helium cover a higher range of temperatures and pressures (compared to JP8/air mixtures) which can be useful for the validation of chemical kinetics mechanisms at high temperatures and pressures.

2. Experimental facility

Experiments have been performed using two constant volume cylindrical and spherical vessels. Fig. 1 shows the general configuration of the experimental set up. The cylindrical vessel is located in a shadowgraph system to take snapshots of flame propagation. The cylindrical vessel is constructed from 316-stainless steel and measures 13.5 cm in diameter and is 13 cm long. The vessel is fitted with 3.5 cm thick fused silica windows at both ends which are sealed to the chamber with o-rings. The windows allow the vessel to operate to a pressure of 50 atm. The purpose of the windows is to provide a clear line of sight through the vessel for a shadowgraph setup that allows real time recording of the combustion event. The vessel is also fitted with band heaters which allow the vessel to be heated up to the initial temperature of 500 K. The images are taken using a CMOS camera capable of capturing up to 40,000 frames per second. The shadowgraph setup consists of five components which are shown in Fig. 2. Starting from the light source, a pinpoint source of light is captured by a spherical mirror 152.4 cm away which reflects the light in a 15.24 cm circular beam which travels through the combustion vessel to the opposite spherical mirror. Once the light beam hits this second mirror it is again focused into a pin point 152.4 cm away onto the CMOS camera. The image that the camera receives with the shadowgraph system is very sensitive to density variation in the media and allows us to see the changes in density of the mixture as the combustion takes place.

The spherical vessel is made of stainless steel which can withstand pressures up to 400 atm. The spherical vessel is constructed from two hemispheres with a diameter of 15.24 cm. It is located in

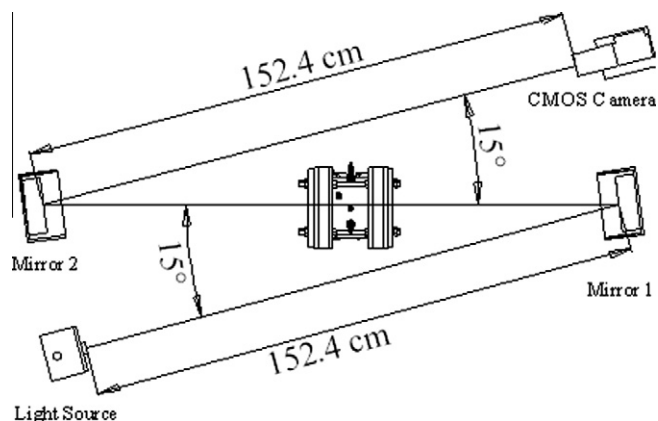


Fig. 2. Shadowgraph system.

an oven which can heat up the vessel up to the initial temperature of 500 K. Both vessels are filled using a control system composed of valves, pipes connected to the required gases, and a vacuum pump. The vessels are filled by the partial pressures method. Liquid fuel is stored in a liquid fuel reservoir which is attached to a liquid fuel manifold. The liquid fuel manifold is equipped with two cartridge heaters to evaporate the liquid fuel. The liquid fuel is heated and is evaporated completely before entering the combustion chamber. The partial pressure of the fuel vapor is measured by an XTE-190-10A Kulite high temperature pressure transducer. The accuracy of this device is such that the errors in the fuel–air equivalence ratio are less than 2%. A computer driven system is used to produce the mixture with the required fuel and oxidizer and to initiate the combustion process. Both vessels are equipped with a Kistler pressure transducer to measure the pressure inside the chamber during the combustion process.

Both vessels are fitted with spark plugs that allow for central point ignition. The energy of ignition for all experiments is 24 mJ. After filling the chamber with fuel, oxidizer, and diluent the system is given at least 5 min to make sure that the mixture is quiescent in

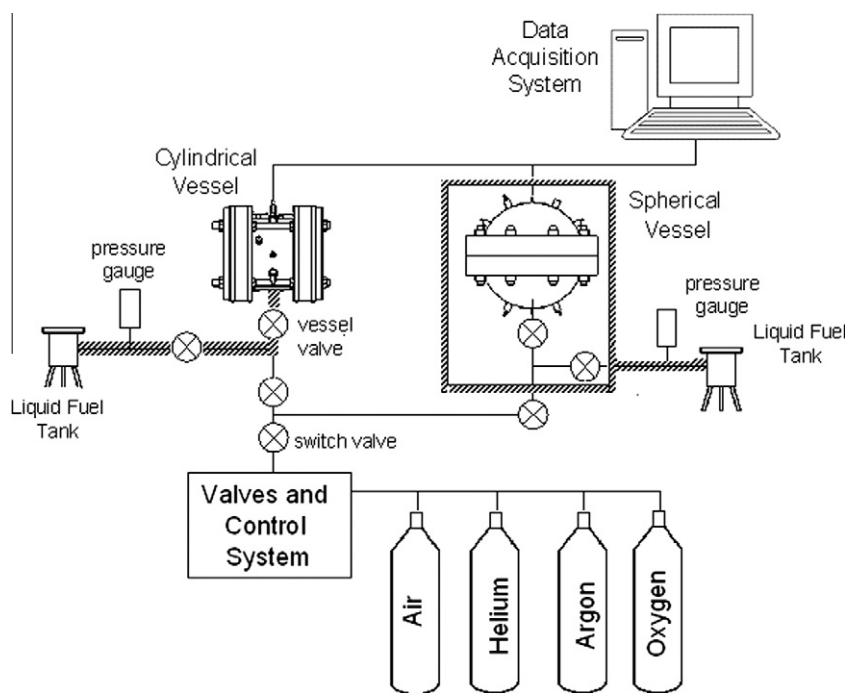


Fig. 1. The sketch of the experimental system.

the chamber. Each experiment was performed at least three times at each operational condition. According to statistical methods, three identical runs are sufficient in order to ensure that the confidence level of the experiment is above 95%. More information about the experimental facilities and procedure of the tests can be found in previous publications [5–7].

2.1. Vapor pressures and temperatures

The fuel used in this study has been provided by the Air Force Research Laboratory (AFRL). The distillation, boiling point and other properties of the applied JP-8 fuel are presented in Table 1. The fuel should be fully vaporized; therefore setting up the proper initial temperature is essential. The initial temperature for all experiments has been fixed at a constant temperature of 493 K. Since the partial pressure of the fuel is very low compared to the partial pressure of oxygen and diluents, the liquid fuel is vaporized completely at this temperature.

2.2. Fuel cracking at high temperatures

In both cylindrical and spherical vessels the temperature of the unburned gases increases due to the propagating flame acting as a piston. In these experiments the temperature range for the unburned gas is approximately 500–700 K. Thermal cracking of the fuel can cause serious errors in the burning speed results, thus it is necessary to determine if there is any thermal cracking of the fuel in this range. Edwards [8] has done several studies on the cracking and deposition of hydrocarbon aviation fuels. An important part of his research concerns the endothermicity of the thermal cracking process of hydrocarbons. He has concluded that for most of these endothermic reacting hydrocarbons, including JP-8, the thermal cracking temperature roughly begins at 750–810 K. In the present study, the unburned gas usually does not exceed 750 K; if it does the corresponding burning speed data are not reported. The thermal cracking process also depends on pressure; it is intensified at higher pressures [8,9]. The important factor in the thermal cracking process is the residence time, which is the average time that the mixture spends as unburned gas. The fuel residence time in this study is estimated by combustion process duration and it is so short (<12 ms) that cracking will not occur [5,10,11].

3. Experimental results and discussion

3.1. Experiments with air and extra diluent gases (EDG)

Experiments with extra diluent gases (14% CO₂ + 86% N₂) have been performed with volumetric percentages of 5% and 10%. Initial conditions were fixed at an initial temperature of 493 K, initial pressures of 1, 2, and 3 atm and equivalence ratios of 0.8, 0.9 and 1. In this study equivalence ratio is defined as the ratio of actual

Table 1
JP-8 fuel properties.

Fuel type	JP-8: 4658 + additives
<i>Distillation</i>	
Initial boiling point (K)	320
10% recovered (K)	426
20% recovered (K)	435
50% recovered (K)	450
90% recovered (K)	481
Final boiling point (K)	498
Flash point (K)	311
Density (kg/L)	0.81
Viscosity (mm ² /s @ 253 K)	2.12
Heat value, heat of combustion (MJ/kg)	42.79

fuel/oxidizer mass ratio to stoichiometric fuel/oxidizer mass ratio ($\phi = (m_{fuel}/m_{oxidizer})_{act}/(m_{fuel}/m_{oxidizer})_{st}$). Table 2 shows the initial conditions of the experiments. The first set of experiments was carried out in the cylindrical vessel to investigate flame structure. All pictures were taken by CMOS camera at 10,000 frames per second with a high resolution. Fig. 3 shows the snapshots of stoichiometric JP-8/air mixtures with three different initial pressures. Fig. 4 shows the snapshots of the burning mixture for three different equivalence ratios at initial pressure of 3 atm. It can be seen that for JP-8/air mixtures increasing the pressure and equivalence ratio enhances the instability. There are some cracks on the flame around the electrodes which are due to the disturbances from the spark electrodes and which develop as the flame grows. The criterion for cell formation is defined as the point when small cells appear on flame surface. This phenomenon takes place simultaneously all over the spherical flame surface. The CMOS camera with high capturing capability and high resolution (512 × 512) can track the beginning of cell formation precisely.

Flame instability originates from the disturbances imposed into the flame by various sources such as spark, interactions with electrodes, density gradient, and stoichiometry gradient in the mixture. These disturbances cause instability if their growth rate is higher than the flame growth rate. The mechanisms which cause and amplify the disturbances define the type of instability. For example, lower heat diffusivity than mass diffusivity in flame amplifies the growth rate of perturbations and leads to thermo-diffusive instability [12–15]. Another type is hydrodynamic (or Rayleigh–Taylor instabilities) in which flame becomes unstable due to disturbances associated with thermal expansion ($\sigma = \rho_u/\rho_b$) [12–15]. The parameter which distinguishes thermo-diffusive instability from hydrodynamic instability is Lewis number ($Le = \alpha/D_m$) which is a non-dimensional parameter. It is the ratio of thermal diffusivity, α , to mass diffusivity, D_m , of deficient reactant in the flame. When $Le < 1$, the observed instability of the flame is thermo-diffusive. Since the transport properties and chemical kinetics mechanism of JP-8 fuel is not developed yet, it is very difficult to calculate the Lewis number of this fuel. However, Lewis

Table 2
Summary of experimental conditions for JP-8/air/EDG mixtures, $T_i = 493$ K.

Test	P_i	ϕ	EDG %
1	1	0.8	0
2	1	0.8	5
3	1	0.8	10
4	1	0.9	0
5	1	0.9	5
6	1	0.9	10
7	1	1	0
8	1	1	5
9	1	1	10
10	2	0.8	0
11	2	0.8	5
12	2	0.8	10
13	2	0.9	0
14	2	0.9	5
15	2	0.9	10
16	2	1	0
17	2	1	5
18	2	1	10
19	3	0.8	0
20	3	0.8	5
21	3	0.8	10
22	3	0.9	0
23	3	0.9	5
24	3	0.9	10
25	3	1	0
26	3	1	5
27	3	1	10

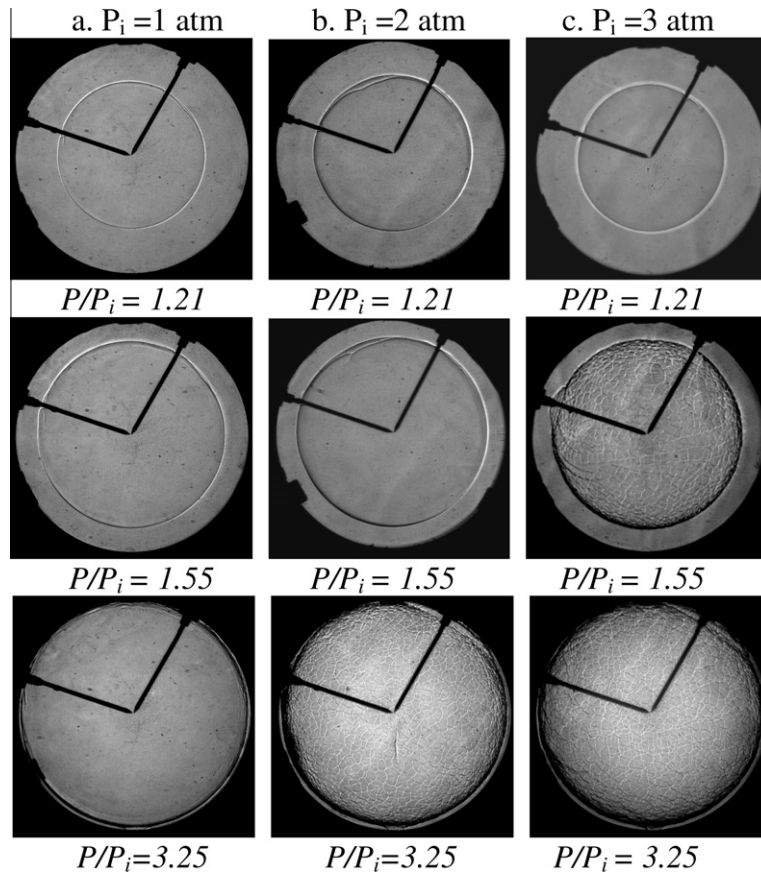


Fig. 3. Snapshots of JP-8/air flames at various initial pressures, $\phi = 1$, $T_i = 493$ K.

number of lean hydrocarbon-air mixtures with more than three carbons is larger than unity [16–19] which suggests that the instabilities observed in our experiments cannot be thermo-diffusive. The other evidence is that thermo-diffusive instabilities usually develop right after ignition, but in hydrodynamic instabilities there is a critical ratio of flame radius to flame thickness after which instability grows; the latter case is observed in our experiments [12,13].

Fig. 3 shows the images of JP-8/air flames at various initial pressures. This figure demonstrates that flame is more sensitive to instability at higher pressures. At higher pressures, flame thickness decreases, which reduces its resistance to perturbations associated with thermal expansion ratio across the flame. In addition to the effect of pressure on flame thickness, Oran and Gardner [20] state that larger pressure pulses increase the amplitude of perturbations in premixed flames. They show that vorticity generation (baroclinic vorticity: $\nabla\rho \times \nabla P/\rho^2$) is stimulated by large pressure pulses along with an abrupt density gradient across the flame which consequently causes cell formation and hydrodynamic instabilities [21,22]. As such, thinner flames result in larger density gradients ($\nabla(1/\rho)$) which boosts vorticity generation. Table 3 shows the critical temperature and pressure corresponding to Figs. 3 and 4 when cellularity starts.

As shown in Fig. 4, flame instability occurs as the equivalence ratio increases. For a heavy hydrocarbon mixture such as JP-8/air, enriching the mixture with fuel causes the deficiency of the light reactant which decreases the Lewis number. In this mixture, as JP-8 is heavier than oxidizer, the light reactant is oxygen. Enrichment also causes earlier instability development.

Fig. 5 shows the effect of EDG on flame structure in flames with an initial pressure of 3 atm, initial temperature of 493 K and three different volumetric percentages of diluents of 0%, 5% and 10% respectively. In these snapshots it is seen that addition of EDG does

not have a major effect on the stability of the flame. Tables 4 and 5 show the cell formation temperatures and pressures at various experimental conditions.

An important issue in these experiments is that cells are formed at large radii; for all of reported cases $r_{cr}/R > 0.5$ where r_{cr} is the radius where cellularity occurs. To understand the role of flame location on instability an attempt was made to normalize the critical radius. The non-dimensional number is the Peclet number (Pe) which is the ratio of flame radius to flame thickness ($Pe = r/\delta$). The critical Peclet number (Pe_c) characterizes the normalized flame radius at which there is a transition to cellularity. To estimate the Pe_c the thickness of flame must be determined. There are several techniques for calculation of δ [13,23,24]. In this study it has been assumed that $\delta = \lambda/\rho c_p S_u$. In this equation, λ is the heat conductivity, ρ is density, c_p is the heat capacity, and S_u is the burning speed. Fig. 6 shows the variation of critical Peclet numbers with equivalence ratios for JP-8/air/EDG mixtures. Fig. 6 shows that for lean JP-8/air mixtures, Pe_c decreases by increasing the equivalence ratio. This figure indicates that as the mixture becomes richer, the flame becomes cellular at smaller radii.

3.2. Experiments with helium and argon

Nitrogen was replaced by helium and argon to investigate the effect on flame structure. Helium and argon have equal molar heat capacities which are smaller than air. Adiabatic flame temperatures of the mixtures with helium and argon are greater than mixtures with air due to the difference in molar heat capacity. Fig. 7 shows the adiabatic flame temperature of stoichiometric JP-8 mixtures with air and $O_2 + He$ versus temperature. In addition, higher values of $\gamma = c_p/c_v$ result in higher temperatures of the unburned gas during the isentropic compression.

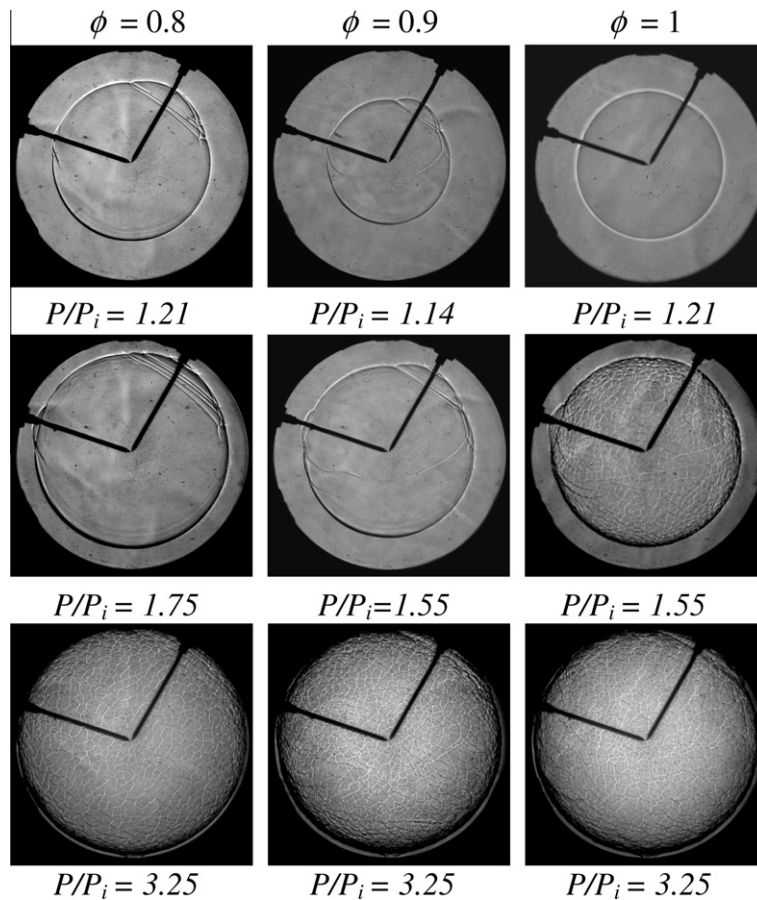


Fig. 4. Snapshots of JP-8/air flames at various equivalence ratios, $P_i = 3$ atm, $T_i = 493$ K.

Table 3
Cell formation analysis of JP-8/air mixtures.

ϕ	$P_i = 1$ atm	$P_i = 2$ atm	$P_i = 3$ atm
0.8	Smooth	Smooth	$P_{cr} \sim 6.1$ atm $T_{cr} \sim 587$ K
0.9	$P_{cr} \sim 4.7$ atm $T_{cr} \sim 705$ K	$P_{cr} \sim 5.1$ atm $T_{cr} \sim 614$ K	$P_{cr} \sim 4.8$ atm $T_{cr} \sim 554$ K
1	$P_{cr} \sim 4.2$ atm $T_{cr} \sim 690$ K	$P_{cr} \sim 4.05$ atm $T_{cr} \sim 583$ K	$P_{cr} \sim 4.1$ atm $T_{cr} \sim 534$ K

Fig. 8 shows the snapshots of JP-8/oxygen/(nitrogen, argon and helium) mixtures at initial temperatures of 493 K and initial pressure of 2.5 atm. It can be seen that argon as diluent is the most destabilizing diluent for flame. Critical pressures of JP-8/oxygen/argon flames are lower than critical pressures of JP-8/oxygen/nitrogen and JP-8/oxygen/helium flames. This can be due to the lower heat diffusivity of argon which can enhance the instability. Helium as diluent is the most stabilizing diluent at higher temperatures and pressures. Compared to argon and nitrogen, helium has the highest heat conductivity and can smooth out and consequently stabilize the flame [25]. Fig. 9 shows JP-8/oxygen/helium flames at initial temperature of 493 K, initial pressure of 4 atm, and at different equivalence ratios. It can be seen that helium increases the stability range of JP-8/oxygen/helium flames compared with JP-8/air/EDG. Table 6 shows the cell formation pressures, temperatures and critical expansion ratios of JP-8/oxygen/helium mixtures at different initial pressures and equivalence ratios. Once again it is demonstrated that the cellularity is strongly dependent on equivalence ratio and pressure. In the case of JP-8/oxygen/helium flames

cell formation occurs at higher temperatures and pressures compared to air.

4. Burning speed measurements

4.1. Burning model

There are several methods used to measure the laminar burning speed [26–31]. The theoretical model used in this work to calculate the burning speed from the pressure rise is based on one previously developed by Metghalchi and Keck [32,33]. Fig. 10 shows a schematic of the model used in this work. The model has been modified to include corrections for energy losses to electrodes and radiation from the burned gas to the wall, as well as the temperature gradient in the preheat zone. It is assumed that gases in the combustion chamber can be divided into burned and unburned gas regions separated by a reaction layer of negligible thickness. The burned gas in the center of chamber is divided into n number of shells where the number of shells is proportional to the combustion duration. Burned gas temperature in each shell is different but all burned gases are in chemical equilibrium with each other. The burned gases are surrounded by a preheat zone (δ_{ph}) having variable temperature, which is itself surrounded by unburned gases. A thermal boundary layer (δ_{bl}) separates the unburned gas from the wall. The effect of energy transfer from burned gas to the spark electrodes is considered by a thermal boundary layer (δ_{bl}). As demonstrated in [5–7], equation of state, volume and energy equations are solved simultaneously:

$$Pv = RT \quad (1)$$

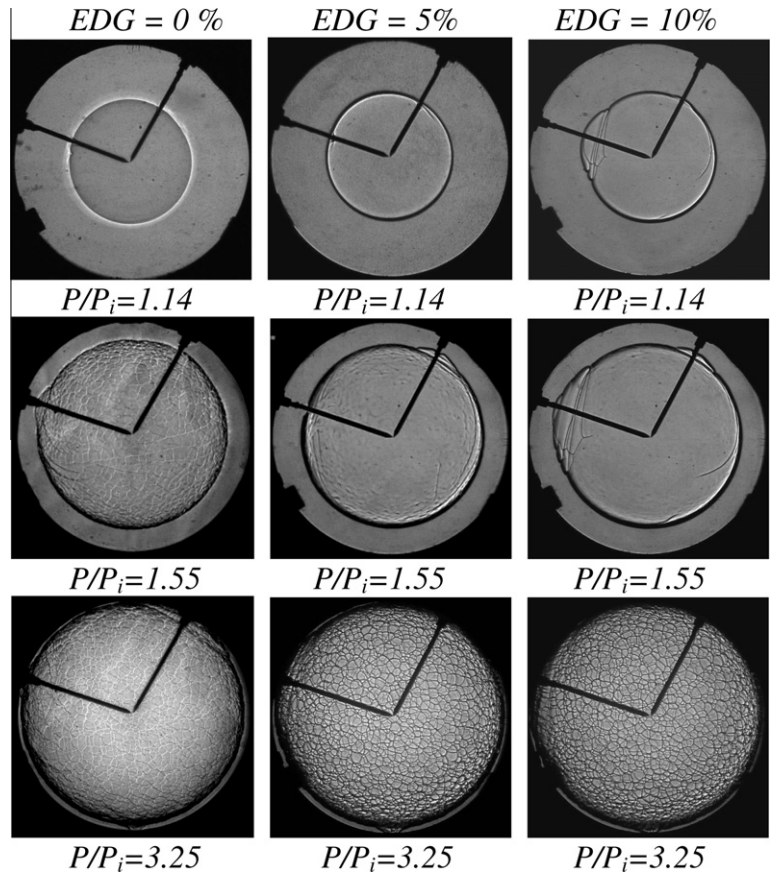


Fig. 5. Snapshots of JP-8/air/EDG flames at several EDG percentages, $\phi = 1$, $T_i = 493$ K, $P_i = 3$ atm.

Table 4
Cell formation analysis of JP-8/air/EDG mixtures (EDG = 5%).

ϕ	$P_i = 1$ atm	$P_i = 2$ atm	$P_i = 3$ atm
0.8	Smooth	Smooth	$P_{cr} = 7.18$ atm, $T_{cr} = 612$ K
0.9	Smooth	$P_{cr} = 4.38$ atm, $T_{cr} = 596$ K	$P_{cr} = 5.1$ atm, $T_{cr} = 547$ K
1	Smooth	$P_{cr} = 3.83$ atm, $T_{cr} = 576$ K	$P_{cr} = 4.06$ atm, $T_{cr} = 515$ K

Table 5
Cell formation analysis of JP-8/air/EDG mixtures (EDG = 10%).

ϕ	$P_i = 1$ atm	$P_i = 2$ atm	$P_i = 3$ atm
0.8	Smooth	Smooth	Smooth
0.9	Smooth	$P_{cr} = 5.32$ atm, $T_{cr} = 631$ K	$P_{cr} = 5.7$ atm, $T_{cr} = 560$ K
1	Smooth	$P_{cr} = 3.77$ atm, $T_{cr} = 575$ K	$P_{cr} = 4.37$ atm, $T_{cr} = 524$ K

In this equation, v is the specific volume and R is the specific gas constant. Pressure is an input to this equation which is measured in the experiments. The mass conservation equation for the burned and unburned gas region is:

$$m = m_b + m_u = \bar{\rho}_b V_b + \bar{\rho}_u V_u = P_i(V_c - V_e)/RT_i \quad (2)$$

where m is the total mass of the chamber, m_b is the mass of the burned gas zone; m_u is the mass of the unburned gas zone. V_c is the volume of the chamber and V_e is the volume of the spark electrodes. In this equation, i denotes the initial conditions, and u and b

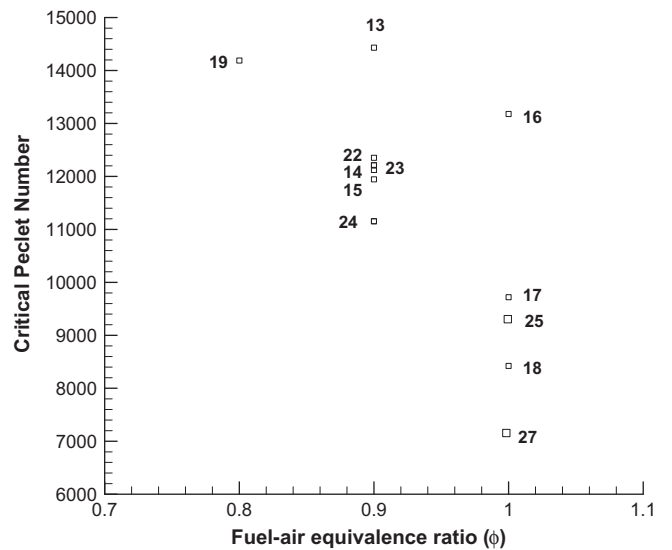


Fig. 6. Critical Peclet numbers (Pe_c) versus equivalence ratio (experimental condition of each number can be found at Table 2).

denote the unburned and burned gas conditions, respectively. $\bar{\rho}$ is the average density and V is the volume of the gas.

The total volume of the gas in the combustion chamber is

$$V_i = V_c - V_e = V_b + V_u \quad (3)$$

The energy conservation equation is

$$E_i - Q_e - Q_w - Q_r = E_b + E_u \quad (4)$$

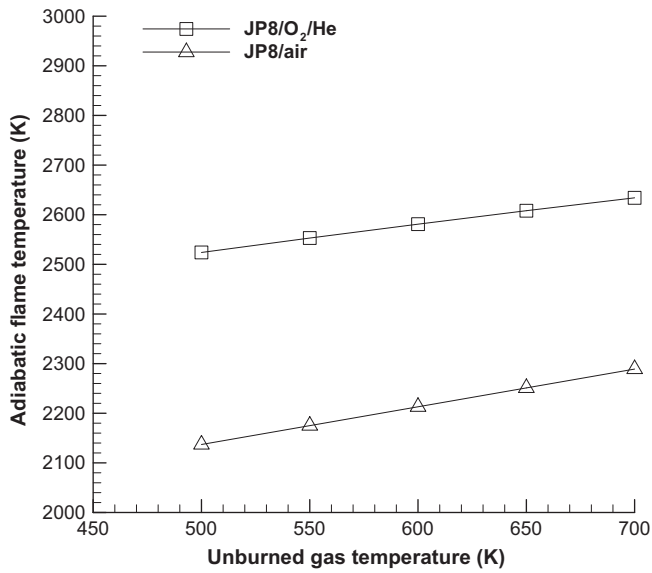


Fig. 7. Adiabatic flame temperature of stoichiometric JP-8/oxygen/diluent mixtures versus unburned gas temperature.

where E_i is the initial energy of the gas, Q_e is the conductive energy loss to the electrodes, Q_w is the energy loss to the wall, Q_r is the radiation energy loss. By using assumptions explained in [5–7], volume and energy equations will be:

$$\int_0^{x_b} (v_{bs}(T', p) - v_{us}) dx' = v_i - v_{us} + (V_{eb} + V_{wb} + V_{ph})/m \quad (5)$$

$$\int_0^{x_b} (e_{bs} - e_{us}) dx = e_i - e_{us} + (PV_{ph}/(\gamma_u - 1) + PV_{eb}/(\gamma_b - 1) + PV_{wb}/(\gamma_u - 1) - Q_r)/m \quad (6)$$

where $v_i = (V_c - V_e)/m$ and $e_i = E_i/m$ are the initial specific volume and energy of the unburned gas in the chamber, v_{bs} is the specific volume of isentropically compressed burned gas, v_{us} is the specific volume of isentropically compressed unburned gas. V_{wb} , V_{ph} and V_{eb} are displacement volume of wall boundary layer, displacement volume of preheat zone ahead of the reaction layer and displacement volume of electrode boundary layer respectively. e_{bs} , e_{us} , and γ_u , are the specific energy of isentropically compressed burned gas, specific energy of isentropically compressed unburned gas and specific heat ratio of unburned gas, respectively. The above equations have been solved for two unknowns: burned mass fraction and the burned gas temperature of the last layer. Given pressure, $P(t)$ as a function of time (measured in the experiments), they can be solved numerically using the method of shells to obtain the burned mass fraction, $x_b(t)$, as a function of time and temperature distribution $T(r, t)$.

Ultimately, the burning speed may be defined as:

$$S_u = \dot{m}_b / \rho_u A_b = m\dot{x} / \rho_u A_b \quad (7)$$

where A_b is the flame area.

All measurements are performed for laminar flames at radii ($r > 4$ cm) to minimize the effects of stretch. In spherical flames the stretch rate is $\kappa = \frac{1}{A} \frac{dA}{dt} = \frac{2}{r} \frac{dr}{dt}$, where r is the radius of the flame.

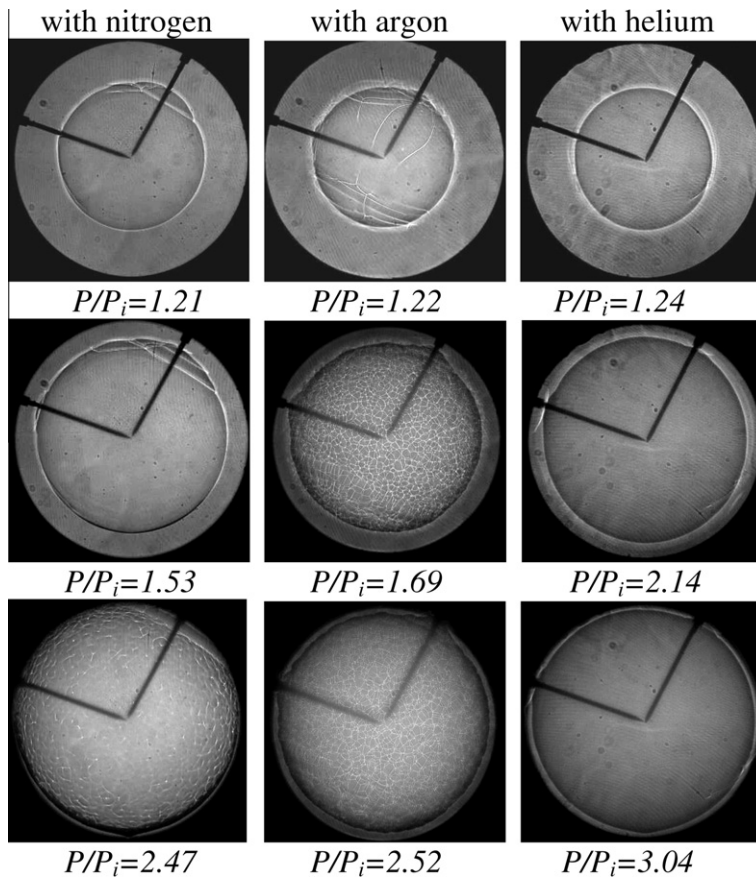


Fig. 8. Snapshots of JP-8/oxygen/diluent flames with different diluents (nitrogen, argon, and helium), $\phi = 1$, $T_i = 493$ K, $P_i = 2.5$ atm.

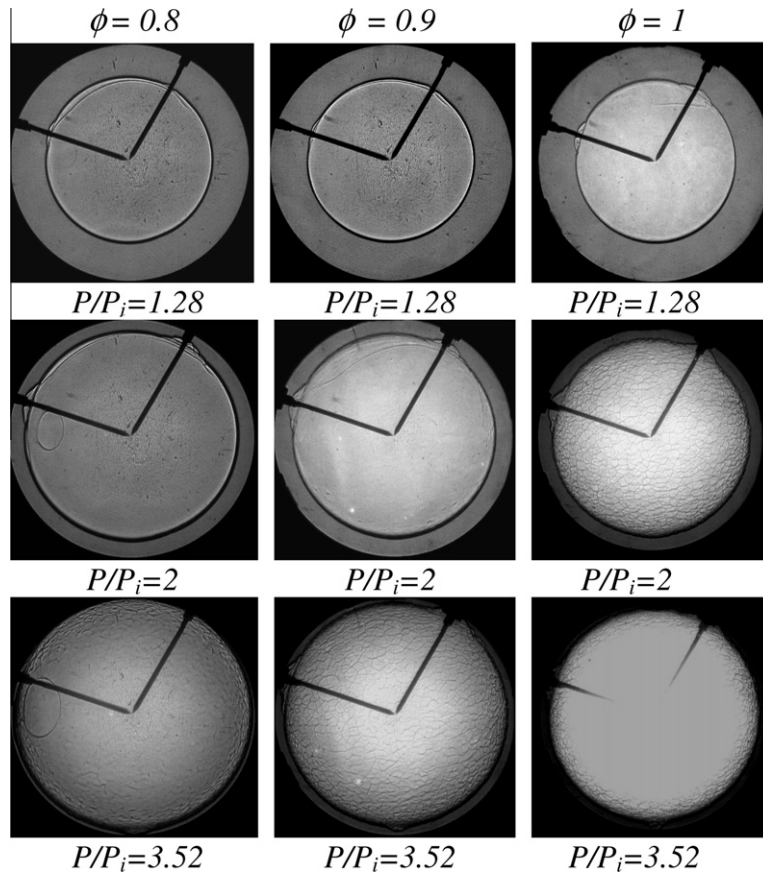


Fig. 9. Snapshots of JP-8/oxygen/helium flames at different equivalence ratios, $T_i = 493$ K, $P_i = 4$ atm.

Table 6
Cell formation analysis of JP-8/oxygen/helium mixtures.

	$P_i = 2$ atm	$P_i = 3$ atm	$P_i = 4$ atm
0.8	Smooth	$P_{cr} = 11.2$ atm $T_{cr} = 709$ K	$P_{cr} = 10.75$ atm $T_{cr} = 640$ K
0.9	Smooth	$P_{cr} = 8.68$ atm $T_{cr} = 658$ K	$P_{cr} = 8.24$ atm $T_{cr} = 606$ K
1	$P_{cr} = 8.04$ atm $T_{cr} = 707$ K	$P_{cr} = 7.33$ atm $T_{cr} = 620$ K	$P_{cr} = 7.59$ atm $T_{cr} = 590$ K

Flame stretch is a phenomenon caused by the variation of flame area versus time. Depending on the conditions, stretch can affect the laminar burning speed values. As the radius of flame increases the stretch rate decreases. In our measurements, flame radii are larger than 4 cm, and stretch effects are negligible. The reported laminar burning speeds in this study are the ones whose corresponding flame stretch rates are lower than 70 1/s. In previous publications we have determined that in this range measured laminar burning speeds are accurate enough that the effects of initial conditions such as spark fire can be neglected [5,34–36].

4.2. Laminar burning speeds

Burning speeds for laminar flames have been measured at high temperatures and pressures. Given the measured values, power law fits have been developed by the least square method to calculate the burning speeds of JP-8/air/EDG and JP-8/oxygen/helium mixtures. For JP-8/air/EDG mixtures, the form of correlation is:

$$S_u = S_{u0}(1 + a_1(1 - \phi) + a_2(1 - \phi)^2) \left[\frac{T_u}{T_{u0}} \right]^\alpha \left[\frac{P}{P_0} \right]^\beta (1 - \text{EDG})^{\theta} \quad (8)$$

where S_{u0} is the burning speed at reference point ($P_0 = 1$ atm, $T_{u0} = 500$ K and $\phi = 1$) in cm/s, ϕ is the mixture fuel–air equivalence ratio, T_u is the unburned gas temperature in K, P is the mixture pressure in atm, and EDG is the diluent mole fraction. This correlation (8) is only valid for smooth (laminar) flames and the range of pressure and temperature depends on smoothness of the flame which is a function of equivalence ratio and diluent type. Fig. 11a shows the range of pressures over which JP-8/oxidizer/diluent flames become cellular. The temperature corresponding to each pressure can be found by following equation:

$$T = T_i(P/P_i)^{(\gamma-1)/\gamma} \quad (9)$$

Table 7 shows the values of the constants in correlation (8).

Fig. 12 shows the laminar burning speeds at three different EDG percentages. This figure shows the measured and fitted values by Eq. (9). It is seen that laminar burning speed decreases as EDG percentage increases. It is likely that the flame temperature decreases due to increasing the heat capacity of the mixture. Regarding the effect of equivalence ratio, there is a consistent behavior in burning speed values. In lean mixtures, laminar burning speed increases by elevating the equivalence ratio. It can be estimated by Fig. 12 that by increasing the EDG fraction by 5%, the laminar burning speed decreases by about 15%. This highlights the importance of EDG in JP-8/air/EDG flames. Addition of EDG to the mixture in internal combustion engines usually decreases the power obtained. The reason can be attributed to slower burning of the mixture which decreases the work production rate. The same procedure of measuring and fitting was done for JP-8/oxygen/helium flames. The power law fit correlation is

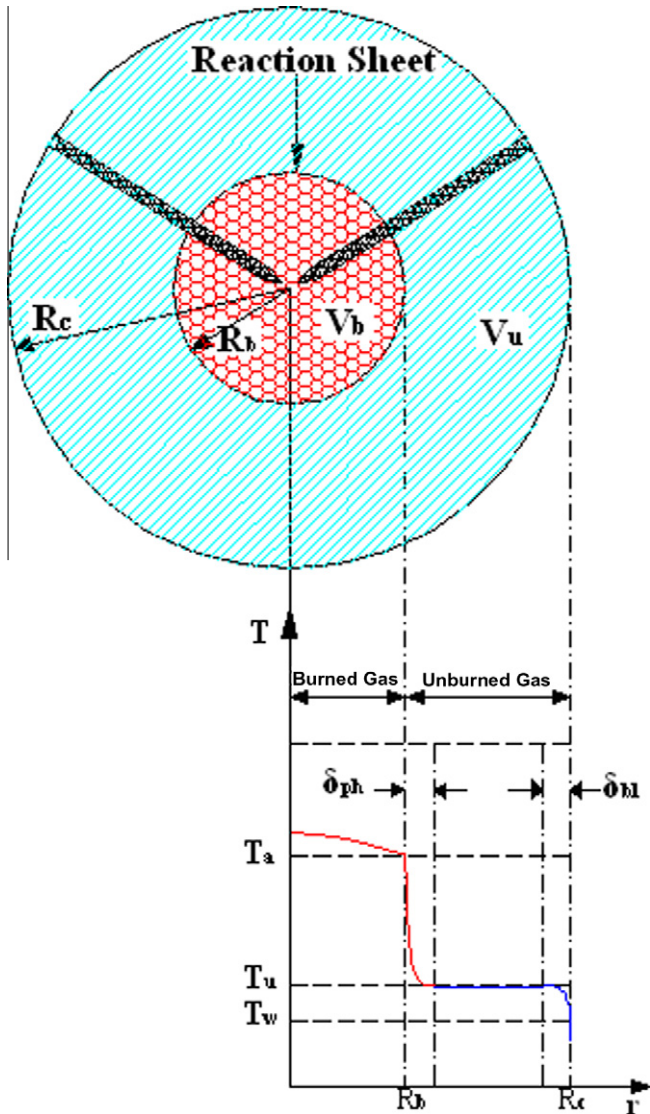


Fig. 10. Schematic of different zones and their corresponding temperatures in the thermodynamics model.

$$S_u = S_{u0}(1 + a_1(1 - \phi) + a_2(1 - \phi)^2) \left[\frac{T_u}{T_{u0}} \right]^\alpha \left[\frac{P}{P_0} \right]^\beta \quad (10)$$

where S_{u0} is the burning speed at reference point ($P_0 = 4$ atm, $T_{u0} = 500$ K and $\phi = 1$). Table 8 shows the values of constants in Eq. (10).

Correlation (10) is only valid for smooth (laminar) flames. Fig. 11b shows the range of pressures over which the flame is smooth. The corresponding temperatures can be calculated using Eq. (9).

Fig. 13 shows the measured and fitted laminar burning speeds of JP-8/oxygen/helium mixtures at initial pressures of 4.5 and 5 atm, initial temperature of 493 K and equivalence ratios of 0.8, 0.9, and 1. The percentage of helium is fixed at a volumetric fraction of 79%. It is observed that laminar burning speeds are tremendously higher than in JP-8/air mixtures. As it is seen in Table 8, the exponents of temperature and pressure, α and β , follow the same trend as those of shown in Table 7. This means that the dependence of the JP-8/oxygen/helium mixture on temperature and pressure is almost the same as JP-8/air/EDG mixtures. The parameter which is remarkably different is S_{u0} . Addition of helium as diluent increases the adiabatic flame temperature which causes

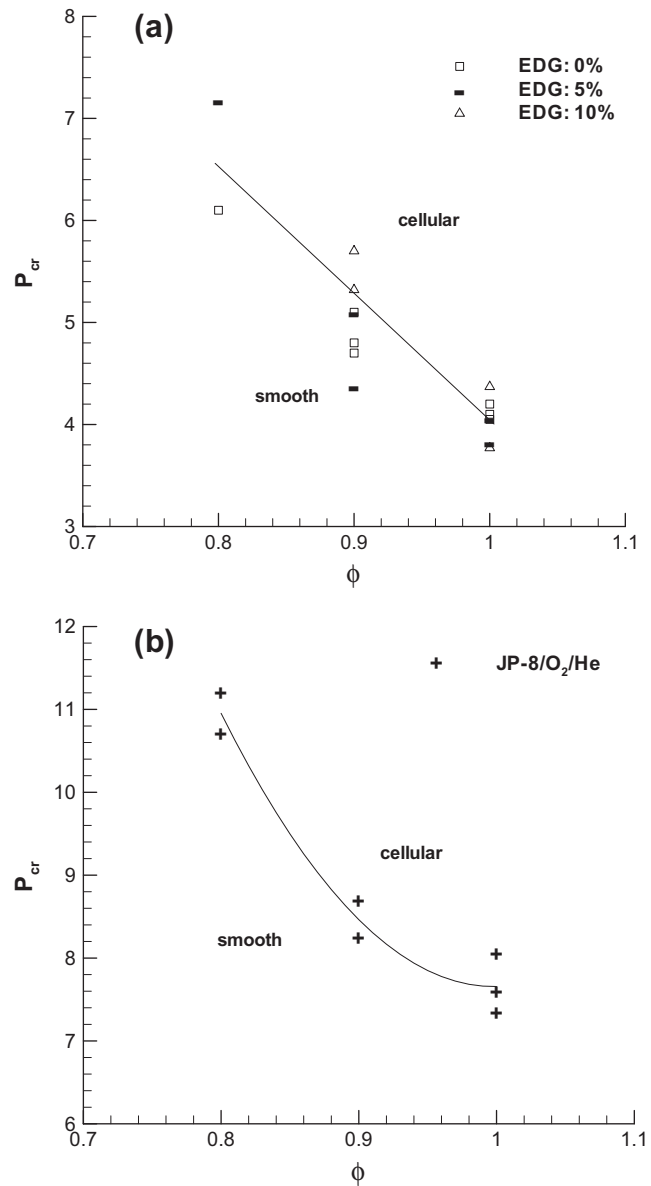


Fig. 11. Cell formation pressure versus equivalence ratio: (a) JP-8/air/EDG and (b) JP-8/oxygen/helium.

Table 7
Power law fit function coefficients of JP-8/air/EDG mixture.

S_{u0} (cm/s)	a	b	α	β	θ
93.63	-0.22	-4.4	2.13	-0.185	3.52

higher reference laminar burning speed. Also laminar burning speed is proportional to the square root of Lewis number ($S_{u0} \sim \sqrt{Le}$). JP-8/oxygen/helium mixtures have higher Lewis numbers because the thermal conductivity of helium is higher than nitrogen. This justifies the higher laminar burning speed of JP-8/oxygen/helium mixtures versus JP-8/air/EDG mixtures.

5. Summary and conclusions

The effect of diluents on flame structure and laminar burning speeds has been studied.

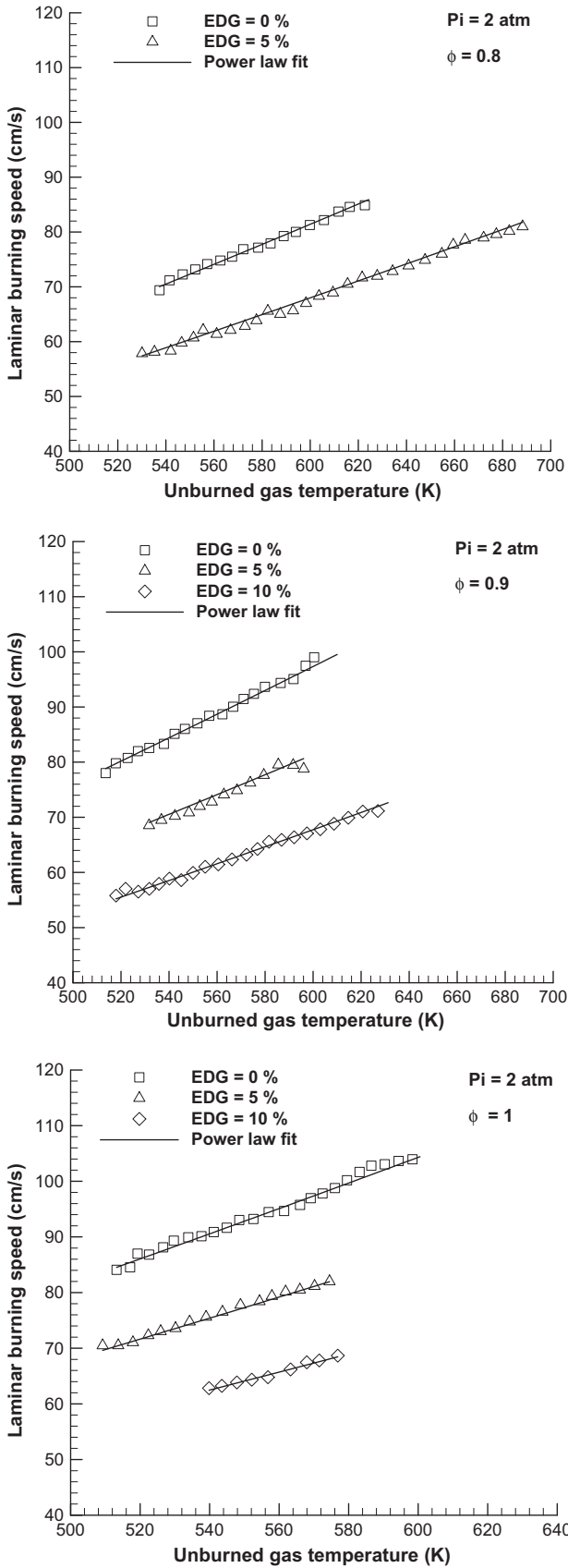


Fig. 12. JP-8/air/EDG laminar burning speeds at various EDG percentages and equivalence ratios, $T_i = 493$ K, $P_i = 2$ atm.

The addition of EDG did not have a major effect on the stability of JP-8/air/EDG flames compared to JP-8/air flames, but it de-

Table 8
Power law fit function coefficients for the JP-8/oxygen/helium mixture.

S_{uo} (cm/s)	a	b	α	β
287.11	-1.38	1.54	2.47	-0.26

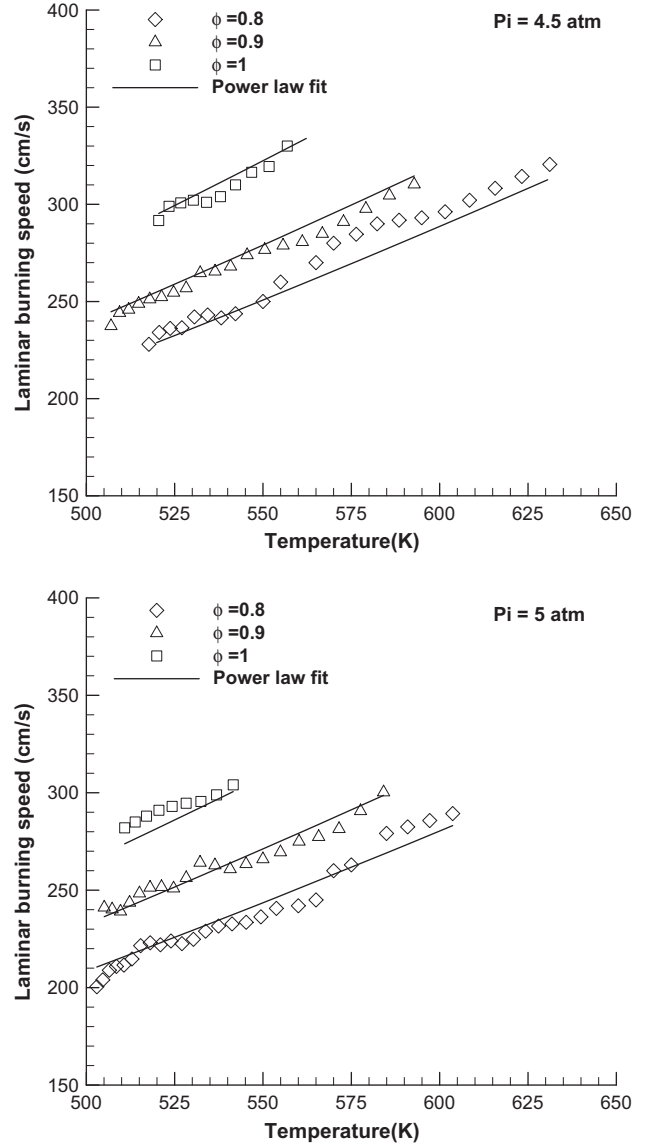


Fig. 13. JP-8/oxygen/helium mixture laminar burning speed at several initial pressures and equivalence ratios, $T_i = 493$ K.

creased the laminar burning speeds due to decreasing the adiabatic flame temperature. It was observed that for a heavy hydrocarbon premixed flame such as for JP-8, increasing pressure causes flame instability. Increasing pressure decreases the flame thickness and reduces the resistance of flame against perturbations associated with expansion ratio. This leads to hydrodynamic instabilities. The other factor which causes flame instability is enriching the mixture in JP-8/air and JP-8/air/EDG mixtures. Peclet numbers of unstable flames were calculated and it was observed that the critical Peclet number is strongly dependent on the equivalence ratio and it decreases by increasing the equivalence ratio. Clearly, it can be concluded that rich mixtures are more vulnerable to perturbations.

A set of experiments were performed with helium and argon as diluents. It was observed that argon causes more instabilities than air. This is because of the lower heat diffusivity of argon compared to air and helium. JP-8/oxygen/helium mixtures have the most stable flames. This is due to their high thermal diffusivities. It was observed in experiments that the JP-8/oxygen/helium flames are stable at higher temperatures and pressures at which JP-8/air and JP-8/oxygen/argon flame were unstable. The laminar burning speeds of JP-8/oxygen/helium flames were measured and it was indicated that helium increases the laminar burning speeds dramatically because of higher adiabatic flame temperatures.

Acknowledgments

This work has been done with the support of the Army Research Office (ARO), Grant No. W911NF0510051, under technical monitoring of Dr. David Mann and Dr. Ralph Anthenien. The authors would like to thank Dr. Tim Edwards, Air Force Research Laboratory (AFRL), for providing the fuels.

References

- [1] Advanced aviation fuels: a look ahead via a historical perspective, Fuel Energy Abstracts, Number 2. March 2002; 43:102.
- [2] Ji C, You X, Holley AT, Wang YL, Egolfopoulos FN, Wang H. Propagation and extinction of mixtures of air with *n*-dodecane, JP-7, and JP-8 jet fuels. In: AIAA 2008-974, 46th AIAA aerospace sciences meeting and exhibit, 7–10 January 2008, Reno, Nevada.
- [3] Kumar K, Sung CJ, Hui X. Laminar flame speeds and extinction limits of conventional and alternative jet fuels. In: 47th AIAA aerospace sciences meeting including the new horizons forum and aerospace exposition, 5–8 January 2009, Orlando, Florida.
- [4] Honnet S, Seshadri K, Niemann U, Peters N. A surrogate fuel for kerosene. Proc Combust Inst 2009;32:485–92.
- [5] Eisazadeh-Far K, Parsinejad F, Metghalchi H. Flame structure and laminar burning speeds of JP-8/air premixed mixtures at high temperatures and pressures. Fuel 2010;89:1041–9.
- [6] Rahim F, Eisazadeh-Far K, Parsinejad F, Andrews RJ, Metghalchi H. A thermodynamic model to calculate burning speed of methane–air–diluent mixtures. Int J Thermodyn 2008;11:151–61.
- [7] Parsinejad F, Arcari C, Metghalchi H. Flame structure and burning speed of JP-10 air mixtures. Combust Sci Technol 2006;178:975–1000.
- [8] Edwards T. Cracking and deposition behavior of supercritical hydrocarbon aviation fuels. Combust Sci Technol 2006;178:307–34.
- [9] Sheu J-C, Zhou N, Krishnan A, Jones AG, Katta VR. Thermal cracking of Norpar-13 under near-critical and supercritical conditions. AIAA Paper 98-3758; 1998.
- [10] Dwards T. Recent research results in advanced fuels. Petrol Chem Devision Preprints 1996;41:481.
- [11] Song C, Lai WC, Schobert HH. Condensed-phase pyrolysis of *n*-tetradecane at elevated pressures for long duration. Product distribution, reaction mechanisms. Ind Eng Chem Res 1994;33:534.
- [12] Kwon OC, Rozenchan G, Law CK. Cellular instabilities and self-acceleration of outwardly propagating spherical flames. Proc Combust Inst 2002;29:1775–84.
- [13] Jomaas G, Law CK, Bechtold JK. On transition to cellularity in expanding spherical flames. J Fluid Mech 2007;583:1–26.
- [14] Sivashinsky GI. Instabilities, pattern formation, and turbulence in flames. Annu Rev Fluid Mech 1983;15:179–99.
- [15] Bechtold JK, Matalon M. Hydrodynamic and diffusion effects on the stability of spherically expanding flames. Combust Flame 1987;67:77–90.
- [16] Bechtold JK, Matalon M. The dependence of the Markstein length on stoichiometry. Combust Flame 2001;127:1906–13.
- [17] Yuan Jiao, Yiguang Ju, Law CK. Pulsating and hydrodynamic instabilities at large Lewis numbers. Combust Flame 2006;144:386–97.
- [18] Sun CJ, Sung CJ, He L, Law CK. Dynamics of weakly stretched flames: quantitative description and extraction of global parameters. Combust Flame 1999;118:108–28.
- [19] Pearlman H. Excitability in high-Lewis number premixed gas combustion. Combust Flame 1997;109:382–98.
- [20] Oran ES, Gardner JH. Chemical–acoustic interactions in combustion systems. Prog Energy Combust Sci 1985;11:251–76.
- [21] Bradley D, Harper CH. The development of instabilities in laminar explosion flames. Combust Flame 1994;99:562–72.
- [22] Clavin P, Williams FA. Effects of molecular diffusion and of thermal expansion on the structure and dynamics of premixed flames in turbulent flows of large scale and low intensity. J Fluid Mech 1982;116:251–82.
- [23] Sun CJ, Sung CJ, He L, Law CK. Dynamics of weakly stretched flames: quantitative description and extraction of global parameters. Combust Flame 1999;118:108–28.
- [24] Poinso T, Veynante D. Theoretical and numerical combustion. Flourown: R.T. Edwards; 2005.
- [25] Sivashinsky G. On the intrinsic dynamics of premixed flames. Philos T Roy Soc A 1990;332:135–48.
- [26] Davis SG, Law CK, Wang H. An experimental and kinetic modeling study of propyne oxidation. In: Twenty-seventh symposium (international) on combustion, Combustion Institute, Boulder, CO; 1998. p. 305–312.
- [27] Dyakov IV, Konnov AA, De Ruyck J, Bosschaart KJ, Brock ECM, De Goeij LPH. Measurement of adiabatic burning velocity in methane–oxygen–nitrogen mixtures. Combust Sci Technol 2001;172:81–96.
- [28] Jerzembeck S, Matalon M, Peters N. Experimental investigation of very rich laminar spherical flames under microgravity conditions. Proc Combust Inst 2009;32:1125–32.
- [29] Konnov AA, Dyakov IV. Measurement of propagation speeds in adiabatic flat and cellular premixed flames of $C_2H_6 + O_2 + CO_2$. Combust Flame 2004;136:371–6.
- [30] Tseng L, Ismail M, Faeth G. Laminar burning velocities and Markstein numbers of hydrocarbon/air flames. Combust Flame 1993;95:410–26.
- [31] Ma L.Z., Chomiak J. Asymptotic flame shapes and speeds of hydrodynamically unstable laminar flames. In: Symposium (International) on Combustion, vol. 27; 1998;545–553.
- [32] Metghalchi M, Keck JC. Laminar burning velocity of propane–air mixtures at high temperature and pressure. Combust Flame 1980;38:143–54.
- [33] Metghalchi M, Keck JC. Burning velocities of mixtures of air with methanol, isooctane, and indolene at high pressure and temperature. Combust Flame 1982;48:191–210.
- [34] Eisazadeh-Far K, Moghaddas A, Al-Mulki J, Metghalchi H. Laminar Burning Speeds of Ethanol/Air/Diluent Mixtures. Proc. Combust. Inst. 2010, doi:10.1016/j.proci.2010.05.105.
- [35] Eisazadeh-Far K, Parsinejad F, Metghalchi H, Keck JC. On flame kernel formation and propagation in premixed gases. Combust Flame 2010;157:2211–21.
- [36] Eisazadeh-Far K, Parsinejad F, Metghalchi H, Keck JC. A thermodynamic model for argon plasma kernel formation. Int J Thermodyn 2010;13:119–25.